LIMNOLOGY and OCEANOGRAPHY

ASLO

Limnol. Oceanogr. 65, 2020, 2912–2925

doi: 10.1002/lno.11562

Photosynthetic energy conversion efficiency in the West Antarctic Peninsula

Jonathan Sherman,[1] **Maxim Y. Gorbunov**,[1] **Oscar Schofield**,[1,2] **Paul G. Falkowski**[1*]

[1]Environmental Biophysics and Molecular Ecology Program, Department of Marine and Coastal Sciences, Rutgers, The State University of New Jersey, New Brunswick, New Jersey

[2]Center for Ocean Observing Leadership, Department of Marine and Coastal Sciences, Rutgers, The State University of New Jersey, New Brunswick, New Jersey

Abstract

The West Antarctic Peninsula (WAP) is a highly productive polar ecosystem where phytoplankton dynamics are regulated by intense bottom-up control from light and iron availability. Rapid climate change along the WAP is driving shifts in the mixed layer depth and iron availability. Elucidating the relative role of each of these controls and their interactions is crucial for understanding of how primary productivity will change in coming decades. Using a combination of ultra-high-resolution variable chlorophyll fluorescence together with fluorescence lifetime analyses on the 2017 Palmer Long Term Ecological Research cruise, we mapped the temporal and spatial variability in phytoplankton photophysiology across the WAP. Highest photosynthetic energy conversion efficiencies and lowest fluorescence quantum yields were observed in iron replete coastal regions. Photosynthetic energy conversion efficiencies decreased by ~ 60% with a proportional increase in quantum yields of thermal dissipation and fluorescence on the outer continental shelf and slope. The combined analysis of variable fluorescence and lifetimes revealed that, in addition to the decrease in the fraction of inactive reaction centers, up to 20% of light harvesting chlorophyll-protein antenna complexes were energetically uncoupled from photosystem II reaction centers in iron-limited phytoplankton. These biophysical signatures strongly suggest severe iron limitation of photosynthesis in the surface waters along the continental slope of the WAP.

Iron availability limits phytoplankton growth and production across ~ 30% of the ocean's surface (Moore et al. 2013). However, iron requirements vary dramatically among species (Ho et al. 2003) and phytoplankton communities may remain relatively iron replete even in regions with extremely low concentrations of iron, such as the South Pacific Gyre (Bonnet et al. 2008). Consequently, there is a need to develop sensitive diagnostic tools for iron limitation in phytoplankton (Hopkinson et al. 2007; Behrenfeld and Milligan 2013). The Southern Ocean has garnered particular interest as it is the world's largest iron-limited region (Boyd 2002; Strzepek et al. 2012).

Over several decades, variable fluorescence signals from photosystem II (PSII) have been used to measure photosynthetic conversion efficiencies. This efficiency, commonly denoted as F_v/F_m, is the quantum yield of photochemistry in PSII (Φ_{PSII}); that is, the ability of absorbed light to drive photosynthetic electron transport from water to a terminal electron acceptor (Kolber et al. 1998). The rate of induction of variable fluorescence on the microsecond time scale can also be used to calculate the effective absorption cross section of PSII (σ_{PSII}) (Kolber et al. 1998; Gorbunov and Falkowski 2005). This latter parameter is a product of the optical absorption cross section of PSII (i.e., the size of the PSII antennae) and the quantum yield of photochemistry in the reaction center (RC) (Ley and Mauzerall 1982; Kolber et al. 1998; Falkowski et al. 2004; Falkowski and Raven 2014).

Fluorescence emission and nonradiative thermal dissipation (with the quantum yields of Φ_F and Φ_T, respectively) compete with photochemistry to dissipate absorbed photons (Butler and Strasser 1977; Butler 1978; Falkowski et al. 2017). The three are complementary, meaning the sum of the three yields is 1.00 (Butler 1978). Moreover, they are remarkably sensitive to the effects of iron limitation on phytoplankton physiology (Lin et al. 2016). Extensive measurements of variable fluorescence under iron limitation have revealed substantial decreases in maximal Φ_{PSII} and pronounced increases in σ_{PSII}. These responses were observed in cultures (Greene et al. 1991; Vassiliev et al. 1995; Strzepek et al. 2012, 2019) and in situ (Greene et al. 1994; Gervais et al. 2002; Suzuki et al. 2002; Behrenfeld and Milligan 2013). Furthermore, shipboard and in situ iron enrichment experiments, revealed

*Correspondence: falko@marine.rutgers.edu

rapid increases in F_v/F_m and decreases in σ_{PSII} following iron amendment (Gervais et al. 2002; Hutchins et al. 2002; Coale et al. 2004; Hopkinson et al. 2007; Moore et al. 2007; Ryan-Keogh et al. 2017).

Low Φ_{PSII} reflects a downregulation in functional RCs, complemented by an increased pool of light harvesting complexes (LHC), some energetically uncoupled from the RCs (Greene et al. 1991; Schrader et al. 2011; Macey et al. 2014). The LHCs that are still coupled energetically serve fewer functional RCs, resulting in an increased σ_{PSII}. With this, phytoplankton economize the high iron quota of RCs (Strzepek et al. 2012). At low light, large LHCs increase excitation energy loss through thermal dissipation and fluorescent emission before being trapped in an active RC (Wientjes et al. 2013). In the Southern Ocean, Strzepek et al. (2019) proposed the low temperatures mitigate this loss. Conversely, at saturating light, the few active RCs are subjected to overexcitation and damage (Greene et al. 1992). To cope, iron-limited phytoplankton increase rapid non-photochemical quenching (NPQ) components (Petrou et al. 2011; Alderkamp et al. 2013). NPQ represents a suite of photoprotective mechanisms activated at high light, effectively increasing Φ_T and simultaneously decreasing σ_{PSII} (Goss and Lepetit 2015; Kuzminov and Gorbunov 2016; Buck et al. 2019). Further work is needed to rapidly assess the occurrence and function of these physiological responses to iron limitation in natural assemblages (Behrenfeld and Milligan 2013). However, for a truly comprehensive evaluation, an additional yield needs to be measured alongside Φ_{PSII}. Previous studies have suggested methods to derive additional yields from variable fluorescence (Hendrickson et al. 2004; Kramer et al. 2004). However, these methods critically depend on a priori assumptions regarding the antenna-RC organization.

To that end, we developed an extremely sensitive, sea-going instrument, PicoLiF (Picosecond Lifetime Fluorescence), which continuously measures in situ chlorophyll fluorescence lifetimes in the picosecond time domain. When the measured lifetimes are normalized to the natural lifetime (15,000 ps, or 15 ns in the case of chlorophyll *a* [Chl *a*]; Brody and Rabinowitch 1957), the result is the quantum yield of fluorescence, Φ_F. As all three quantum yields sum to unity, direct measurements of Φ_{PSII} and Φ_F allow quantification of Φ_T by difference (Lin et al. 2016) and the fraction of energetically uncoupled LHC-RC complexes (Park et al. 2017). In addition, they provide insight into regulation of energy transfer (Buck et al. 2019) and photoprotection (Kuzminov and Gorbunov 2016) in PSII. In the oceans, Φ_F varies about fivefold in response to light and nutrients (Lin et al. 2016). Indeed, the direct measurement of Φ_F from lifetimes in the picosecond time domain is the only way to calibrate or verify remotely sensed Φ_F, which is a highly derived product (Huot et al. 2005; Behrenfeld et al. 2009; Lin et al. 2016).

Here, we evaluated surface phytoplankton photophysiology in the West Antarctic Peninsula (WAP). In this region, a cross shelf iron gradient exists, hypothesized to control phytoplankton abundance and productivity (Annett et al. 2017). Custom-built fluorometers were deployed during the 2017 annual WAP Long Term Ecological Research cruise in the austral summer. A FIRe (Fluorescence Induction and Relaxation) instrument measured F_v/F_m, σ_{PSII}. Simultaneously, the PicoLiF instrument measured fluorescence lifetimes. We hypothesized our combined measurements would reveal a distinct iron-limited physiology, with significantly higher Φ_T, and an increased pool of uncoupled LHC-RC in the WAP offshore waters.

Materials and methods

Study area

Data were collected on board the ASRV Laurence M. Gould. Sampling was carried out along perpendicular cross shelf transects spaced 100 km apart. The study region corresponds to the LTER project grid lines 100–600 (Waters and Smith 1992) (Fig. 1). Following Steinberg et al. (2015), we differentiate between three subregions across the WAP: the shallow coastal region, the continental shelf, and the deep continental slope roughly 200 km offshore.

Sample collection and analysis

Sampling stations were at 20 km intervals along each grid line. Samples were collected for Chl *a* and dissolved inorganic nutrients (nitrate, phosphate, and silicate) following Carvalho et al. (2019). Variable fluorescence and fluorescence lifetime data were collected continuously from surface waters (~ 5 m) while underway with FIRe and PicoLiF fluorometers respectively, as described by Lin et al. (2016). The instruments used flow through cuvettes connected to the ship's surface water intake pump. The water passed through two de-bubblers prior to entering the cuvette.

Mixed layer depth (MLD) was defined as the depth at which the maximum buoyancy frequency was observed in CTD profiles, following Carvalho et al. (2017). The critical depth was calculated from surface daily integrated photosynthetically available radiation (PAR), collected from the mast of the ship (QSR-240P, Biospherical Instruments) and the light attenuation coefficient (K_{PAR}) calculated from the empirical relationship of K_{PAR} and Chl *a* concentration, as proposed by Sverdrup (1953) and Nelson and Smith (1991). Night and day were differentiated using NOAA's solar calculator (https://www.esrl.noaa.gov/gmd/grad/solcalc/).

Photophysiology

We recorded variable fluorescence using a mini-FIRe instrument as previously described (Gorbunov and Falkowski 2005; Kuzminov and Gorbunov 2016). Variable fluorescence was induced by a saturating single turnover flash (STF) from blue light-emitting diodes (450 nm with 30 nm half bandwidth), which cumulatively reduce all PSII RCs within ca. 100 μs. This excitation protocol results in minimum and maximum fluorescence yields (F_0 and F_m). The quantum yield of photochemistry in PSII was then calculated as $(F_m-F_0)/F_m = F_v/F_m$

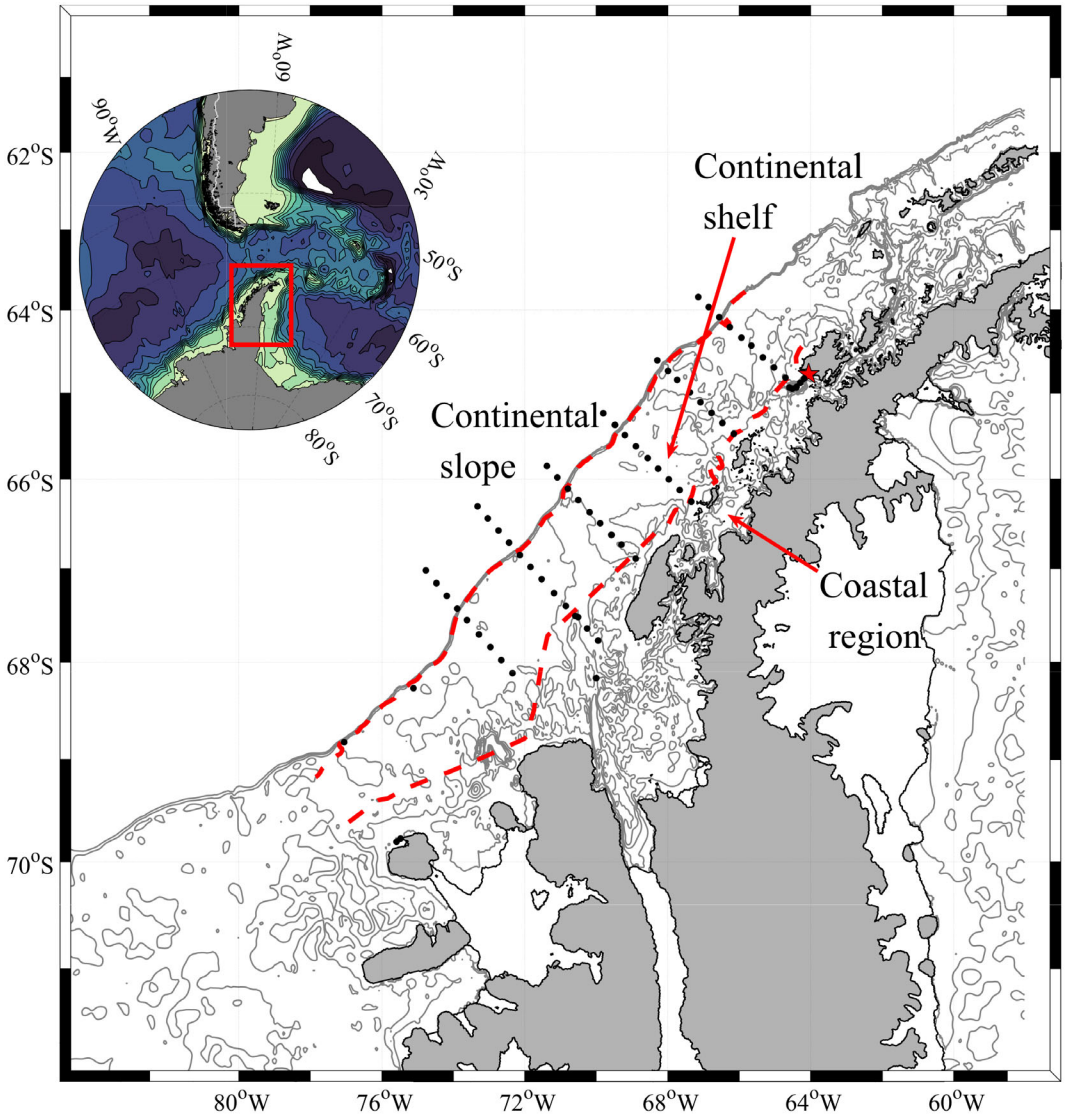

Fig 1. West Antarctic Peninsula (WAP) Long Term Ecological Research (LTER) site. Insert at top left shows the WAP in relation to South America. Black dots on main figure represent the sampling stations along the 100 line in the south to the 600 line in the north. Red dashed lines denote the three subregions along the WAP; the coast, the continental shelf and the continental slope. Red star is the location of the U.S Palmer station on Anverse Island. Bathymetry in figure and insert is from ETOPO1 dataset.

(Butler 1978; Kolber et al. 1998). The effective absorption cross section of PSII, σ_{PSII} (at 450 nm), is calculated by fitting the fluorescence rise to a cumulative one-hit Poisson function (Ley and Mauzerall 1982).

Every ~ 30 min the flow through on the mini-FIRe was automatically paused in order to conduct slow fluorescence irradiance (FE) curves. These were used to retrieve electron transport rates (ETR) as a function of irradiance and to characterize the state of phytoplankton photoacclimation to their short- and long-term light history (Falkowski 1994; Ralph and Gademann 2005). During FE curves, the water sample was trapped in the cuvette for ca. 10 min and then exposed to increasing PAR levels (0–800 μmol photons m^{-2} s^{-1}) with an actinic blue light source (450 nm). Every light step lasted 30–40 s to promote short-term acclimation to each new PAR level, followed with standard measurements. FE curves in this study are termed slow as light steps were longer than other comparable studies, where light steps lasted 10–20 s (Serôdio et al. 2006; Suggett et al. 2015). This was done, as the acclimation is slower at lower water temperatures. From FE curves, we calculated the rate of photosynthetic electron transport normalized per PSII RC (ETR_{PSII}, with units of e^- s^{-1} RC^{-1}), as a function of PAR (Gorbunov et al. 2000, 2001) from

$$ETR_{PSII} = E \times \sigma_{PSII} \times \left[\left(\Delta F'/F'_m \right) / \left(F_v/F_m \right) \right] \quad (1)$$

Here, E is irradiance, F_v/F_m and σ_{PSII} are measurements in the dark (PAR = 0), respectively. $\Delta F'/F'_m$ is the quantum yield

of photochemistry at a given PAR level, with the prime notation indicating measurement under ambient light ($\Delta F' = F'_m - F'$, where F' is a steady-state fluorescence at a given light step). FE curves were than fitted to a hyperbolic tangent function to derive maximal ETR through PSII (ETR_{PSII}^{max}), and the E_K value (saturating light level) following Jassby and Platt (1976) as

$$ETR_{PSII} = ETR_{PSII}^{max} \times \tanh(E/E_K) \quad (2)$$

Picosecond fluorescence decays, measured with the PicoLiF, were deconvoluted from the instrument response function and fitted to a sum of three exponentials with a custom TCSPFIT Matlab package utilizing a Nelder-Meade simplex algorithm (Enderlein and Erdmann 1997). Φ_F was then calculated from

$$\Phi_F = \tau/\tau_0 \quad (3)$$

where τ is the measured lifetime and τ_0 is the natural lifetime of Chl *a* (Brody and Rabinowitch 1957; Brody 2002). The natural lifetime is the time that would be required for a molecule to return to the ground state from an excited state if fluorescence were the sole dissipation pathway. For Chl *a*, τ_0 is 15 ns and is constant, independent of solvent, organism or environmental condition (Brody and Rabinowitch 1957; Brody 2002; Lakowicz 2006). We then calculated the quantum yield for thermal dissipation (Φ_T) as

$$\Phi_T = 1 - \left[\frac{F_v}{F_m} + \frac{\tau}{\tau_0}\right] \quad (4)$$

All fluorescence measurements were corrected for the blank signal measured routinely from filtered seawater (0.2 μm) (Bibby et al. 2008). To minimize changes in temperature, the flow through system relies on thick walled tubing for insolation.

In the current setup, phytoplankton experienced ~ 10 min of low-light acclimation from the time they entered the ship's underway system to when the FIRe and PicoLiF measurements were conducted. In this time frame, most of the rapid NPQ mechanisms (e.g., xanthophyll cycling) relax, leading to a recovery in F_v/F_m. However, this time is not sufficient to alleviate the effects of photoinhibition, which requires > 10 min to recover (Alderkamp et al. 2013). Considering this, our standard measurements represent a state in which phytoplankton are not in an entirely low-light acclimated state. In effect, this means that F_v/F_m may be slightly underestimated when the measurements are conducted during the day. This issue is more pertinent for the calculation of ETR, as the underlying assumption relies on a truly low-light acclimated baseline (Eq. 1). As there is an additional low-light acclimation period before a FE curve is measured the deviations mentioned above would decrease. In any case, from Eq. 1 it can be seen that underestimating F_v/F_m and σ_{PSII} results in an underestimation of ETR. To minimize any under- or overestimations, preferential weight is given to data collected during the night. Although data collected during the day may cause some issues in interpretation, we argue that the low-light acclimation periods used here are sufficient nonetheless to provide distinct differences in the photophysiological status of phytoplankton in response to iron and light availability in this region.

Statistical analyses

The average of each photophysiological variable reported in this paper represents the median value. The median was chosen because each individual variable was not normally distributed and included statistical outliers. To describe the deviation from the median, we calculated the median absolute deviation, a robust measure of dispersion around the median (Leys et al. 2013). For improved spatial comparison of variables, surface maps were produced using a Locally Weighted Scatter-plot Smoother. Significance with a $\rho \leq 0.05$ was determined from Pearson's linear correlation.

Results

WAP physical and chemical setting

Surface concentrations of Chl *a* ranged from 0.06 to 16.9 mg m^{-3}. Surface Chl *a* concentration significantly correlated with distance to shore (Table 1), with higher concentrations along the coast, decreasing offshore over the continental shelf and slope (Fig. 2a). Macronutrients were replete along the entire grid, with increasing nitrogen (as nitrate) and phosphate over the slope (Fig. 2b,c). Furthermore, N/P ratio tracked closely with the canonical 16/1 Redfield ratio, indicating that nitrogen and phosphate were not limiting factors in this region. Silicate, a crucial nutrient for diatoms, also decreased but was still abundant nonetheless (Fig. 2d). Overall, our data support the notion that along the WAP, oceanic conditions transition over a short distance (~ 200 km), from a coastal- to an HNLC-ecosystem over the continental slope, where previous studies indicate iron depletion (Annett et al. 2017).

Table 1. Pearson's linear correlation coefficients matrix between independent variables (surface PAR and distance to shore) and dependent variables (F_v/F_m, fluorescence lifetime, Φ_T, σ_{PSII}, surface Chl *a* concentration, and ETR_{max}^{PSII}). All coefficients are significant ($\rho \ll 0.05$).

	Surface PAR	Distance to shore
F_v/F_m	−0.444	−0.614
Fluorescence lifetime	−0.481	0.644
Φ_T	0.435	0.653
σ_{PSII}	−0.237	0.624
Surface Chl *a* conc.	0.089	−0.406
ETR_{PSII}^{max}	0.522	0.319

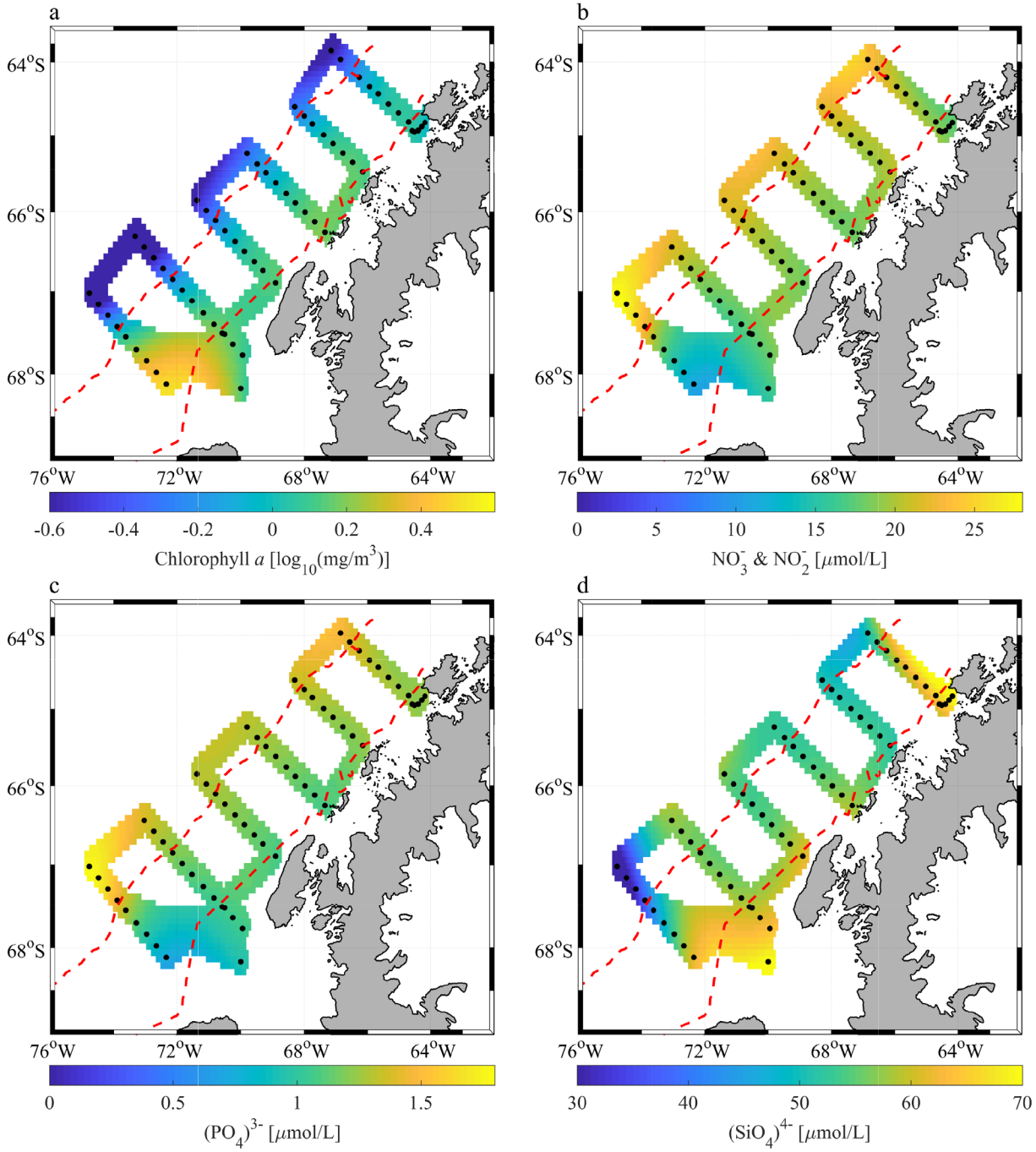

Fig 2. Surface distribution maps of; (**a**) Chl *a*, (**b**) nitrate and nitrite c-phosphate, and (**d**) silicate. Data collected from CTD rosette cast or underway water collection, denoted by black dots. Red dashed lines highlight the borders between the WAP coast, shelf and slope regions. Note that Chl *a* is presented on a logarithmic scale to accommodate a range in orders of magnitude.

Spatial variability in photophysiological parameters

Surface maps of F_v/F_m, fluorescence lifetimes, σ_{PSII} and Φ_T show clear gradients across the continental shelf (Fig. 3; Table 2). The differences are significant, showing the highest degree of correlation with distance from shore (Table 1). As seen in Table 2, throughout a diel cycle, F_v/F_m values along the coast were relatively high (0.42 ± 0.06), and progressively decreased by up to 50% offshore along the shelf (0.3 ± 0.08) and slope (0.22 ± 0.04). Fluorescence lifetimes, in contrast, increased offshore. Along the coast fluorescence, lifetimes were relatively low, 0.77 ± 0.07 ns, increasing to 1.03 ± 0.17 ns along the shelf and 1.29 ± 0.23 ns along the slope. Consequently, Φ_T increased from 0.5 ± 0.05 along the coast, to 0.62 ± 0.06 and 0.69 ± 0.04 at the shelf and slope.

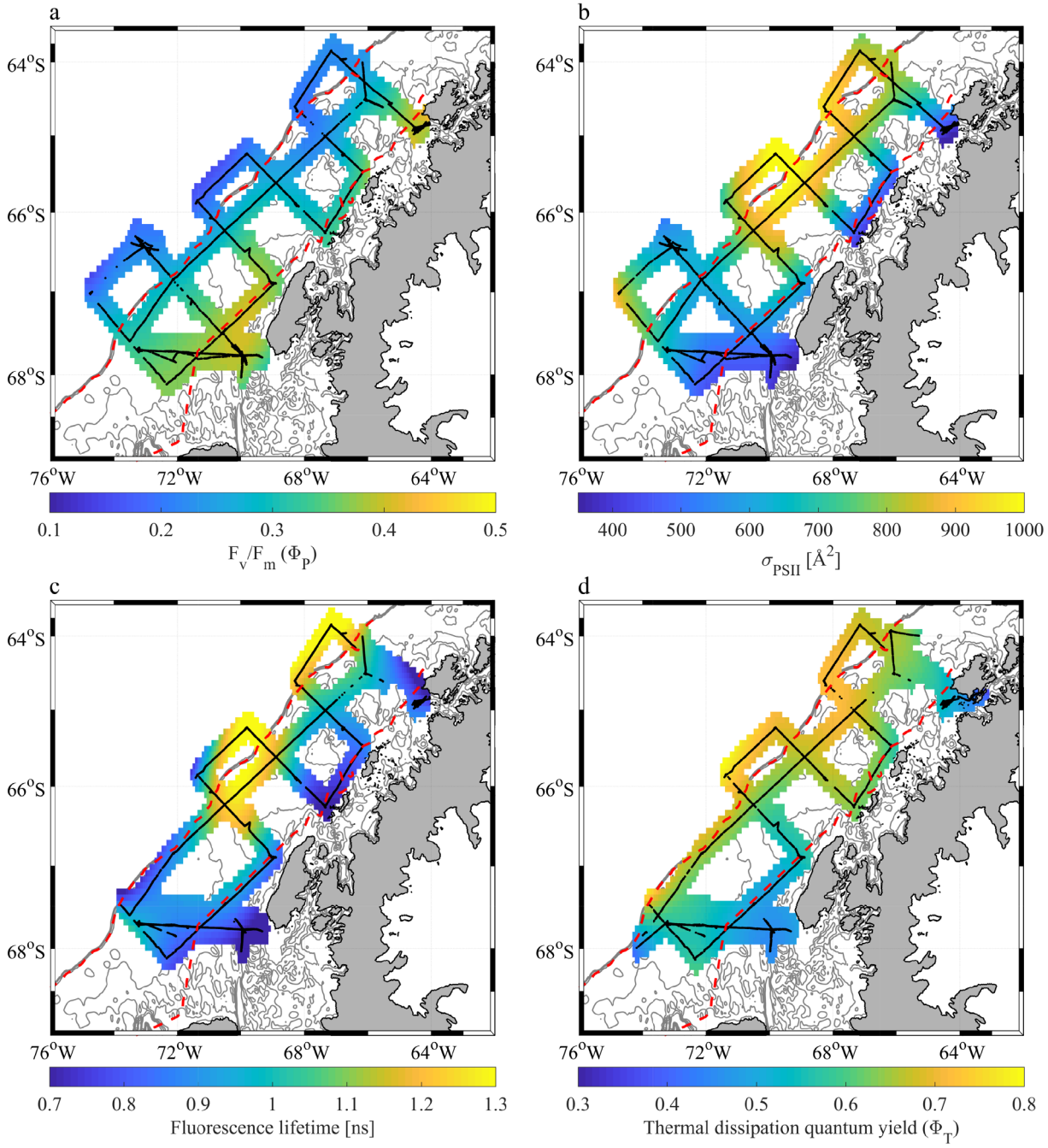

Fig 3. Surface distribution maps of; (**a**) F_v/F_m, (**b**) σ_{PSII}, (**c**) fluorescence lifetime, and (**d**) thermal dissipation quantum yield (Φ_T). F_v/F_m and σ_{PSII} collected from underway FIRe measurements. Fluorescence lifetime collected from underway PicoLiF measurements. Φ_T calculated from Eq. 4. Black dots denote measurement locations. Red dashed lines highlight the borders between the WAP coast, shelf and slope regions.

Similarly, σ_{PSII} increased from 484 ± 54 Å^2 along the coast to 694 ± 132 Å^2 over the shelf, reaching 760 ± 168 Å^2 at the slope. Likewise, diel averaged ETR^{PSII}_{max} rates progressively increased from 58 ± 107 e$^-$ s^{-1} RC^{-1} along the coast to 137 ± 55 and 230 ± 105 e$^-$ s^{-1} RC^{-1} out over the shelf and slope (Table 2).

Diel variability in photophysiological parameters

Both F_v/F_m and fluorescence lifetimes displayed a pronounced diel cycle throughout the WAP (Fig. 4), negatively correlated with surface PAR (Table 1). Median F_v/F_m values during the night across the whole grid were 0.38 ± 0.1, concurrent with an average fluorescence lifetime of

Table 2. Median and median absolute deviation of photophysiological parameters; F_v/F_m, σ_{PSII}, fluorescence lifetime, Φ_T, and ETR^{PSII}_{max}. Data were parsed by location; coast, shelf and slope, and by time; night or day.

		Night	Day	Full diel cycle
F_v/F_m	Coast	0.48 ± 0.03	0.39 ± 0.07	0.42 ± 0.06
	Shelf	0.35 ± 0.07	0.27 ± 0.08	0.3 ± 0.08
	Slope	0.24 ± 0.03	0.19 ± 0.04	0.22 ± 0.04
	Full grid	0.38 ± 0.1	0.29 ± 0.1	0.31 ± 0.1
σ_{PSII} [Å^2]	Coast	476 ± 42	492 ± 58	484 ± 54
	Shelf	710 ± 142	678 ± 125	694 ± 132
	Slope	792 ± 174	744 ± 162	760 ± 168
	Full grid	588 ± 126	564 ± 120	568 ± 124
Fluorescence lifetime (ns)	Coast	0.81 ± 0.08	0.76 ± 0.1	0.77 ± 0.09
	Shelf	1.11 ± 0.13	0.97 ± 0.18	1.03 ± 0.17
	Slope	1.5 ± 0.06	1.07 ± 0.21	1.29 ± 0.23
	Full grid	1.03 ± 0.21	0.84 ± 0.15	0.9 ± 0.17
Φ_T	Coast	0.46 ± 0.02	0.53 ± 0.05	0.5 ± 0.05
	Shelf	0.58 ± 0.06	0.65 ± 0.07	0.62 ± 0.06
	Slope	0.66 ± 0.02	0.72 ± 0.09	0.69 ± 0.04
	Full grid	0.53 ± 0.08	0.61 ± 0.09	0.59 ± 0.09
ETR^{max}_{PSII} ($e^- s^{-1} RC^{-1}$)	Coast	58 ± 15	119 ± 37	107 ± 39
	Shelf	59 ± 17	176 ± 53	137 ± 55
	Slope	208 ± 118	263 ± 100	230 ± 105
	Full grid	64 ± 21	149 ± 53	128 ± 55

1.03 ± 0.21 ns. During the day, as light intensity increased, F_v/F_m decreased by ~ 20% to 0.29 ± 0.1, while fluorescence lifetimes decreased to 0.84 ± 0.15 ns. Conversely, Φ_T increased from 0.53 ± 0.08 to 0.61 ± 0.09 between night and day (Table 2). A weak negative correlation between σ_{PSII} and PAR intensities was seen (Table 1). However, despite this, a diel cycle was not a prominent feature, particularly along the coast (Fig. 5d; Table 2), and σ_{PSII} values during the night and day averaged 588 ± 126 Å^2 and 564 ± 120 Å^2, respectively (Table 2). On the other hand, ETR^{PSII}_{max} correlated positively with PAR (Table 1). During the night ETR^{PSII}_{max} was low (64 ± 21 $e^- s^{-1} RC^{-1}$), while during the day ETR^{PSII}_{max} more than doubled (149 ± 53 $e^- s^{-1} RC^{-1}$) (Table 2).

Discussion

Our results reveal a clear gradient in photophysiological characteristics across the continental margin of the WAP (Fig. 3; Table 2). This gradient is consistent with bottom-up control by iron availability in surface waters and supports the hypothesis that iron strongly limits phytoplankton photochemical energy conversion offshore (Annett et al. 2017; Schofield et al. 2018). The combination of variable fluorescence and lifetimes revealed an increased amount of uncoupled LHC complexes under iron limitation (Fig. 6) as well as a clear tradeoff between photochemistry and thermal dissipation (Fig. 7), resulting from the spatial gradient in iron stress across the WAP. To support this conclusion, we discuss a number of physiological responses to iron limitation across the WAP. These include spatial variabilities in nighttime values and diel cycles of photophysiological parameters, LHC-RC uncoupling, and Φ_T. In addition, we examine the variability in ETR^{PSII}_{max}.

At night, when NPQ is nil (Lin et al. 2016), F_v/F_m over the continental slope decreased by 50% in comparison to the iron richer regions closer to the coast (Table 2). At the same time, fluorescence lifetimes and σ_{PSII} increased by 85% and 65%, respectively. These trends are diagnostic of iron stressed photosynthesis along the continental slope. The extremely high values of σ_{PSII} offshore corroborate previous laboratory measurements on iron-limited Southern Ocean species (Strzepek et al. 2019). Diel cycles of photophysiological parameters were similar across the WAP, with a nighttime maxima and midday minimum (Fig. 5). However, the magnitude of diel variations was much larger in iron-limited regions (Fig. 5; Table 2). The diel cycles observed in the iron-limited WAP continental slope contrast with previously established signatures of iron limitation observed in the Equatorial Pacific (Behrenfeld and Kolber 1999). In that region, dominated by cyanobacteria, F_v/F_m decreased by 35–60% following the sunset and recovered at sunrise, resulting in a pillared nighttime feature. Behrenfeld and Kolber (1999) concluded this diel fluorescent pattern was due to state transitions in iron-limited plankton.

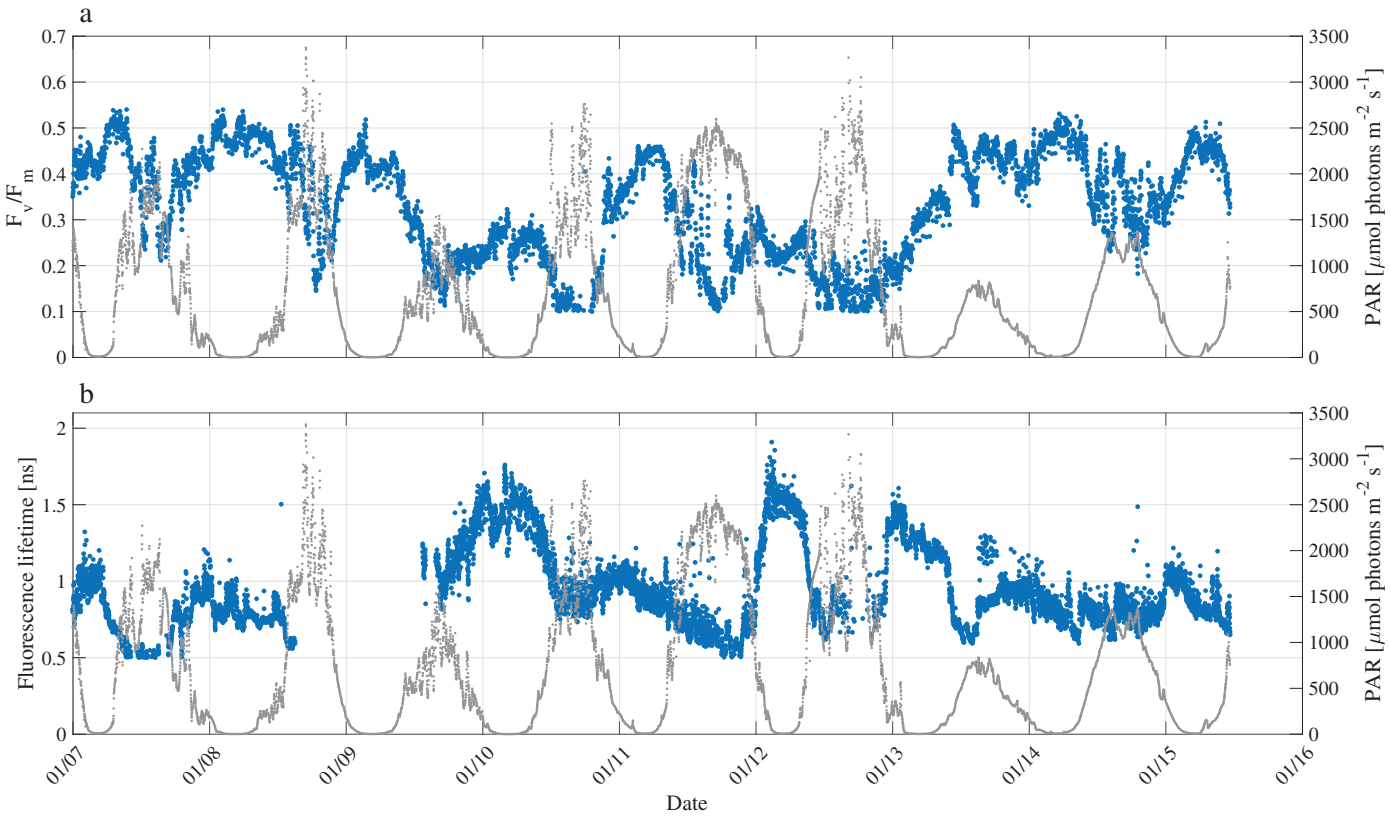

Fig 4. Diel cycles in (**a**) F_v/F_m (blue) and (**b**) fluorescence lifetime [ns] (blue) on the left Y axis from underway FIRe and PicoLiF measurements. Right Y-axis shows atmospheric PAR intensity (gray dots) as measured from the ships mast. Data represent the first week of the cruise.

Such diel patterns were not observed in iron-limited regions in the WAP (Figs, 4, 5). This is because phytoplankton assemblages in the WAP are dominated by diatoms (Schofield et al. 2017), in which state transitions are absent (Owens 1986).

We next consider the occurrence of energetically uncoupled LHC complexes. The basic biophysical model for energy distribution in the photosynthetic unit predicts an inverse relationship between low-light acclimated Φ_{PSII} and Φ_F (Butler 1978; Lin et al. 2016; Falkowski et al. 2017). The correlation between F_v/F_m and fluorescence lifetime collected at night validates our assumption of linearity in these two yields (Pearson's linear correlation coefficient of −0.91, $\rho < 0.05$). However, the data are not consistent with Butler's model (Fig. 6). To calculate the fraction of uncoupled LHC complexes, the relationship between F_v/F_m and fluorescence lifetime was modeled for three physiological states with different lifetimes (Park et al. 2017). Two states represent cases in which LHC complexes are coupled to RCs and RCs are fully open or fully closed with lifetimes of 0.5 and 1.5 ns, respectively. The third represents uncoupled LHCII complexes with a very long lifetime of 4 ns (Palacios et al. 2002). The presence of such energetically detached antenna complexes would ultimately lead to longer measured lifetimes, and these lifetimes may exceed the values observed for fully closed RCs (~ 1.5 ns).

In Fig. 6, nighttime F_v/F_m values are plotted against lifetimes. A distinct deviation from the classical inverse relationship predicted by Butler's model is seen at the low F_v/F_m. Moreover, two clusters are clearly seen. The first cluster represents coastal data, with high F_v/F_m, low fluorescence lifetimes and small σ_{PSII}. This coastal cluster aligns fairly well with the modeled case for open RC with nearly fully coupled antenna complexes, as expected for iron-replete conditions. The second cluster represents data from the continental slope, with low F_v/F_m and long fluorescence lifetimes. This analysis suggests that 20–30% of antenna complexes are detached in iron-limited waters offshore.

Over the WAP slope, Φ_T significantly increased (Fig. 3d; Table 2), confirming our hypothesis that phytoplankton increase Φ_T as iron limitation intensifies. At night, in the absence of NPQ, Φ_T along the slope was ~ 45% higher than in coastal waters (Table 2). This increase in Φ_T is driven by a reduction in the photosynthetic use efficiency. With few active RC, and a significantly large and uncoupled LHC, excitons are more likely to dissipate as heat (Strzepek et al. 2019). In addition to the positive correlation with distance to shore, Φ_T also positively correlated with increasing light availability (Table 1). During the day, Φ_T increased by an additional 15% across the WAP (Table 2), yet offshore values were still ~ 40% higher than onshore values. This daytime increase in Φ_T indicates NPQ activation that effectively increases thermal dissipation. As

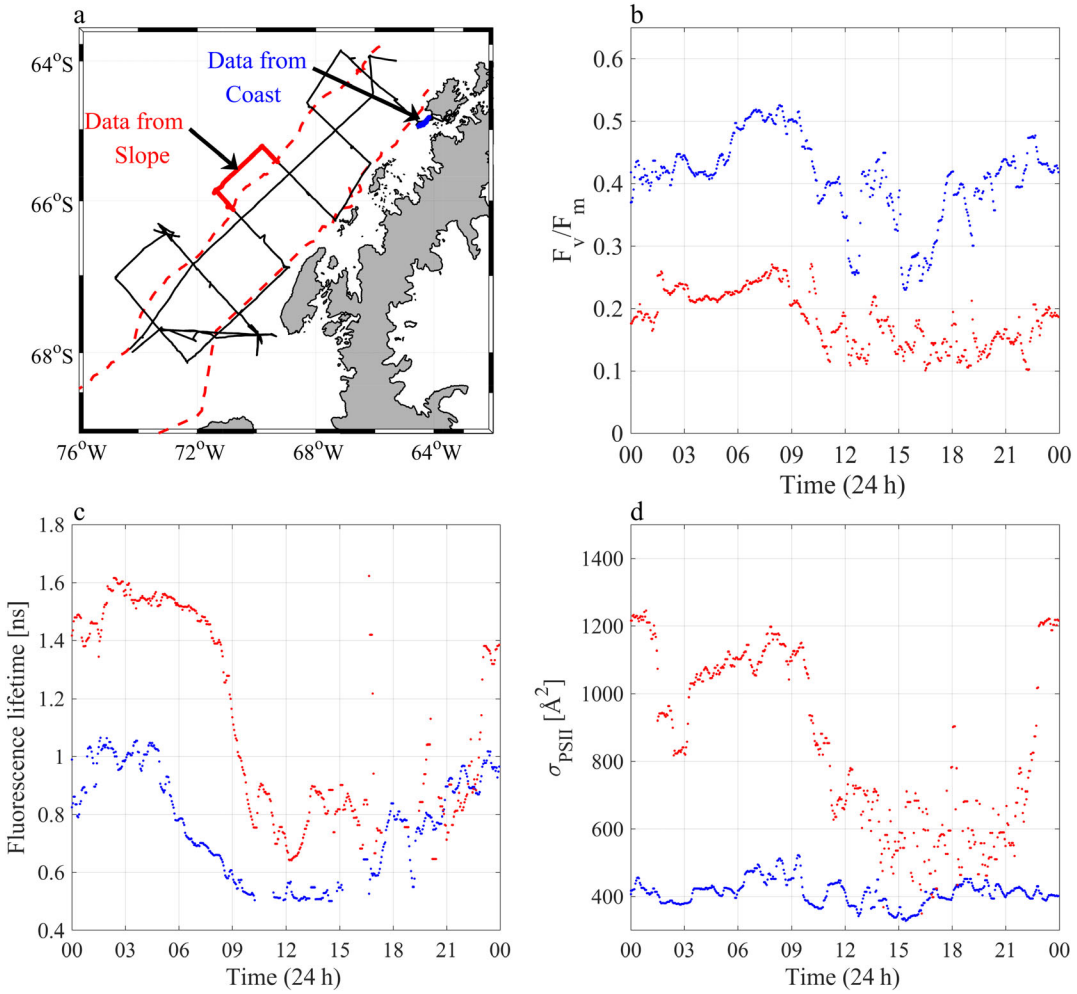

Fig 5. A comparison of diel cycles in phytoplankton photophysiology over the coast, in blue, and continental slope, in red. (**a**) Locations in which the data plotted were collected. (**b**) F_v/F_m, (**c**) fluorescence lifetime, and (**d**) σ_{PSII}.

iron-stressed phytoplankton are more prone to photooxidative damage at the active RCs (Greene et al. 1992; Strzepek et al. 2012), increasing Φ_T acts to further decrease excitation pressure on the RC in favor of thermal dissipation in the uncoupled antenna complex. To examine this hypothesis, we plotted the relationship between F_v/F_m and thermal dissipation from the full dataset (Fig 7). A liner regression revealed a slope of −0.94 (r^2 = 0.98); the deviation from a −1.00 slope is attributed to ca. 6% dissipation by fluorescence (Lin et al. 2016). The increased Φ_T observed in the WAP supports recent studies showing higher photoprotective capacities in iron-limited phytoplankton assemblages (Alderkamp et al. 2013; Schallenberg et al. 2020).

Moreover, the increase in uncoupled complexes combined with exceptionally high Φ_T offshore strongly agrees with the proposed mechanism for efficient NPQ in diatoms. This mechanism attributes the rapid NPQ capacity to thermal dissipation in the LHC, driven by xanthophyll pigment cycling and the presence of Lhcx proteins (Lepetit et al. 2017; Buck et al. 2019). These presumably cause a conformational change that distances the antenna complex from the RC, increasing the Föster resonance energy transfer distance, functionally mediating the energetic uncoupling of the LHC and RC.

Lastly, we turn to evaluate possible light limitation in the WAP surface waters, a second, potentially important bottom-up control in this region (Moline 1998). Increased photoprotective activity during the day across the WAP, inferred from Φ_T (Table 2), suggests that phytoplankton are exposed to saturating light intensities in the near-surface layer. Combined with the high ETR^{PSII}_{max} values measured during the day (Table 2), it is highly unlikely that surface phytoplankton were light limited.

Although ETR^{PSII}_{max} was initially assessed in regard to light limitation, it was surprising and perhaps counterintuitive to observe significantly higher (~120%) ETR^{PSII}_{max} in the iron-limited waters offshore (Table 2). A similar response in ETR^{PSII}_{max} to iron limitation has been reported in phytoplankton assemblages from the Northeast subarctic Pacific, where iron

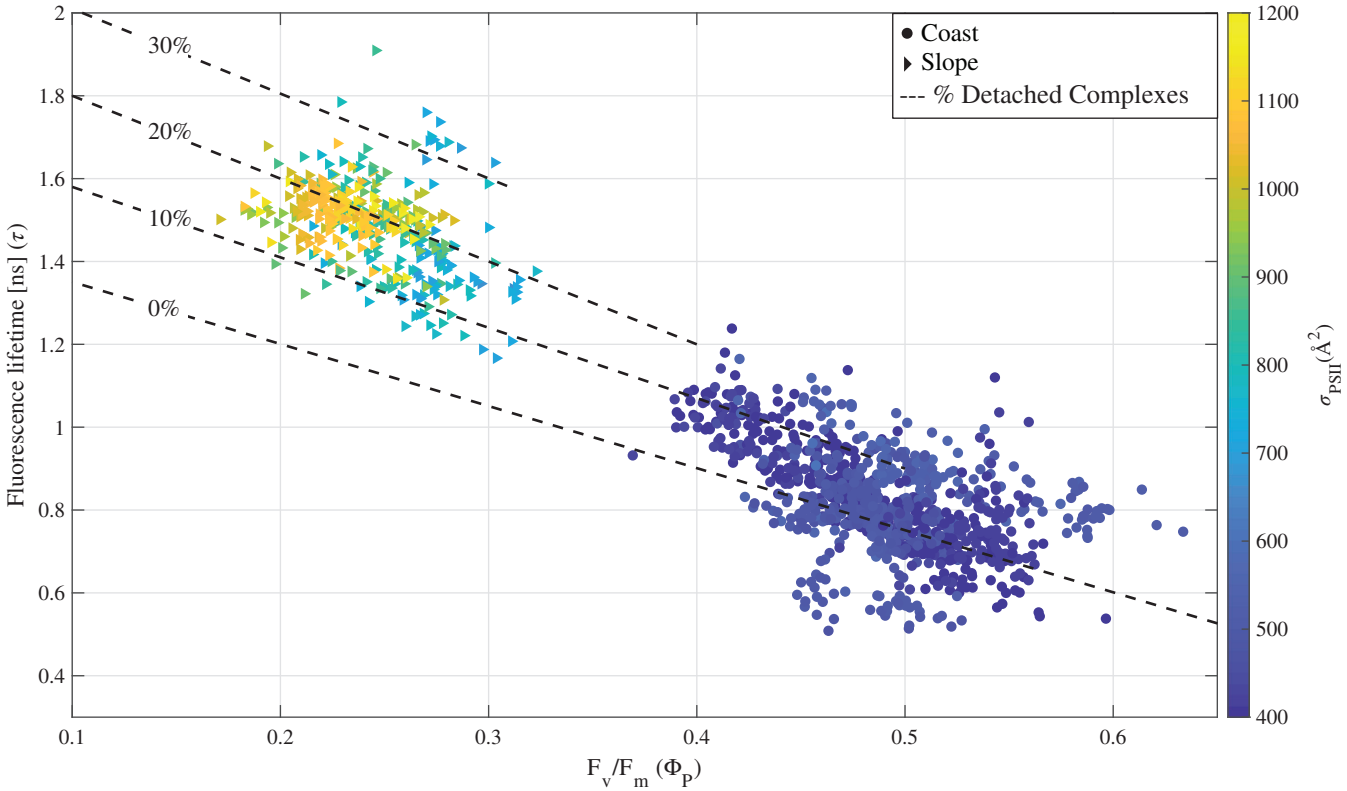

Fig 6. Relationship between F_v/F_m, fluorescence lifetime and σ_{PSII} (in color bar). Circles represent data collected from the coast and triangles data from the slope. In both locations, only data collected during the night are shown in order to remove the nonlinear effect of NPQ on the otherwise linear relationship between F_v/F_m and fluorescence lifetime (Lin et al. 2016). Dashed lines indicate the fraction of uncoupled reaction centers. 0% dashed lines represents the modeled linear dependency of F_v/F_m and fluorescence lifetime (Butler 1978). 10–30% dashed lines represent the dependency of these parameters in detached antenna PSII reaction centers complexes.

amendment experiments resulted in decreased ETR^{PSII}_{max} (Schuback et al. 2015). Similar results were seen in laboratory experiments with the diatom *Thalassiosira oceanica*, the haptophyte *Chrysochromulina polylepis* (Schuback et al. 2015), and the cyanobacterium *Synechococcus sp*. (Blanco-Ameijeiras et al. 2018). The iron-limited increase in ETR^{PSII}_{max} is assumed to be an additional effect of the iron economizing physiology. In this manner, more excitons are funneled from the large antenna to fewer functional RC, leading to increased ETR per active PSII RC, each associated with a larger σ_{PSII}. While we argue that our data provide little evidence for light limitation in the surface waters we measured, and is supported by previous studies (Moline et al. 1996), the effect of the MLD on light availability in the water column cannot be overlooked. Indeed, along the coast, MLD (13.3 ± 5.1) nearly reached the critical depth (14.9 ± 8.4 m), while along the slope, the MLD exceeded by up to ~30% the critical depth (30 ± 6 and 22.9 ± 10.9 m, respectively). Sverdrup's critical depth hypothesis (Sverdrup 1953) appears to imply that light limitation is particularly severe in the water column along the continental slope. Why then, is there little photophysiological evidence for light limitation in the surface waters offshore? We speculate that our data agree with the hypothesis that in Southern Ocean phytoplankton, the photophysiological response to iron limitation eliminates the antagonistic co-limitation of iron and light (Strzepek et al. 2012). Accordingly, the high capacity for light harvesting in the iron-limited slope community alleviates light limitation. On the other hand, in the iron replete coastal community, light limitation is more probable and agrees with a recent study along the coast (Carvalho et al. 2019). Still, during the day coastal phytoplankton in the surface waters themselves experience light saturating conditions. This may result from a long-term acclimation to limiting light conditions in the water column, subjecting phytoplankton to overexcitation at saturating light, likely only met at the surface.

Our analysis assumes a uniform taxonomic composition across the WAP, which can potentially influence fluorescence measurements (Suggett et al. 2009). This is a fairly safe assumption as HNLC regions are anomalous in this respect, yet with relatively consistent fluorescence signatures across taxa (Suggett et al. 2009). This is further supported in Southern Ocean species (Strzepek et al. 2019), in particular diatoms, the dominant species in the WAP (Schofield et al. 2017).

Data presented here provide strong evidence for a distinct gradient in the degree of iron limitation across the WAP

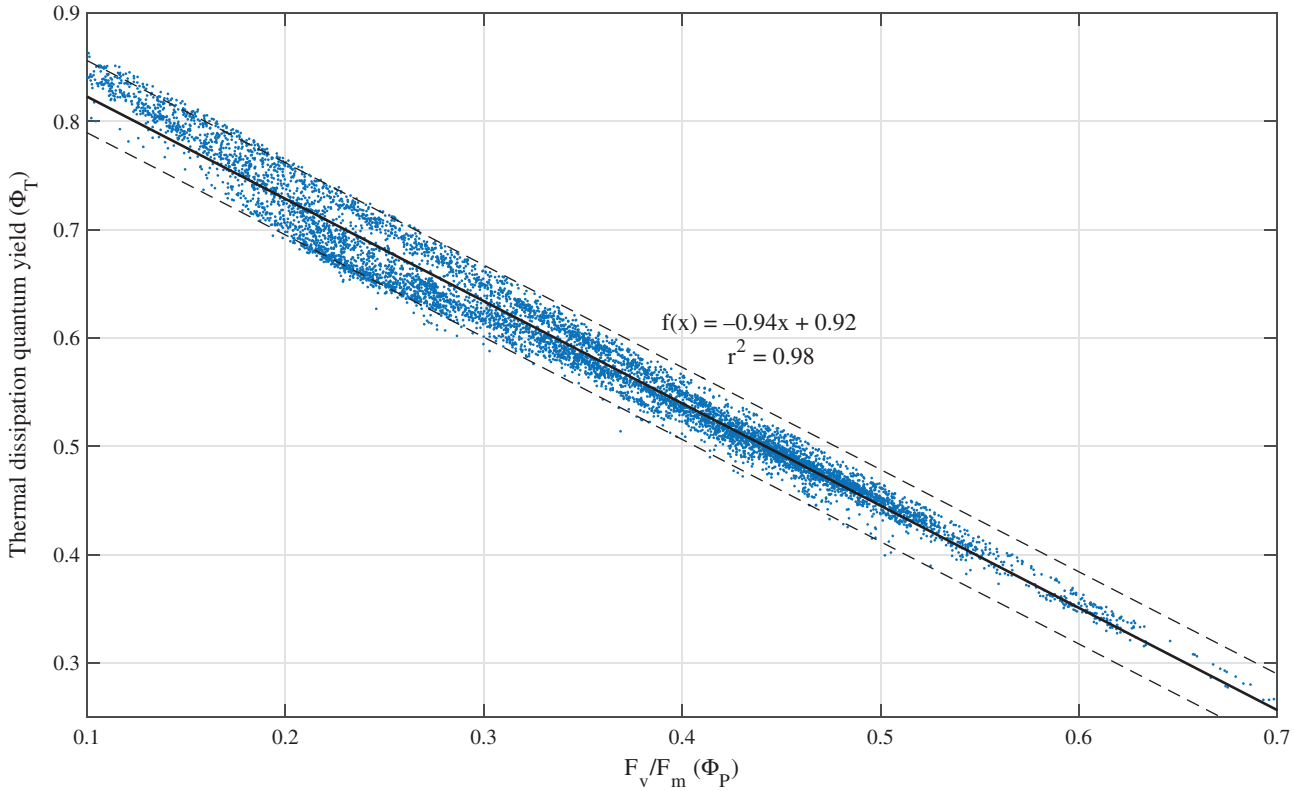

Fig 7. Relationship between F_v/F_m and the quantum yield of thermal dissipation (Φ_T). The quantum yield of thermal dissipation is calculated from underway measurements of variable fluorescence with a FIRe instrument and fluorescence lifetime with a PicoLiF instrument as $\Phi_T = 1 - \left[\left(\frac{Fv}{Fm}\right) + \left(\frac{\tau}{\tau_0}\right)\right]$, where τ is the measured lifetime in ns and τ_0 is the natural lifetime of Chl *a*, 1.5 ns (*see* main text). A linear regression line, the 95% confidence interval, the regression equation, and the r^2 are indicated ($n = 7590$).

during the summer. Iron limitation was shown to be minimal at the coast and severe further offshore. As we hypothesized, combined measurements of Φ_{PSII} and Φ_F showed increased fractions of uncoupled LHC-RC complexes as well as clear increases in Φ_T resulting from iron stress. The deep MLD across the WAP may have caused light limitation in the water column. Nonetheless, the clear acclimation to iron stress in the surface waters along the slope effectively reduced potential light limitation to a degree that phytoplankton were more susceptible to light saturation. Our in-depth analysis of strictly biophysical mechanisms in response to iron stress is highly supported by a large number of studies, further strengthening our conclusions.

The WAPs case study, presented here, highlights the potential of our coupled Φ_{PSII} and Φ_F measurements as a rapid diagnostic tool for in situ assessments of iron limitation at high spatial and temporal resolution. More critically, this diagnostic tool provides a unique new avenue to assess in situ the role of uncoupled complexes in natural assemblages, their effect on satellite retrieved chlorophyll fluorescence and primary productivity models.

DATA AVAILABILITY STATEMENT

Nutrient and Chlorophyll data are available through Palmer LTER Datazoo (https://oceaninformatics.ucsd.edu/datazoo/catalogs/pallter/datasets). Underway Fire and PicoLiF data deposited at https://seabass.gsfc.nasa.gov/.

References

Alderkamp, A., M. Mills, G. van Dijken, and K. Arrigo. 2013. Photoacclimation and non-photochemical quenching under in situ irradiance in natural phytoplankton assemblages from the Amundsen Sea. Antarctica. Mar. Ecol. Prog. Ser. **475**: 15–34. doi:10.3354/meps10097

Annett, A. L., J. N. Fitzsimmons, M. J. M. Séguret, M. Lagerström, M. P. Meredith, O. Schofield, and R. M. Sherrell. 2017. Controls on dissolved and particulate iron distributions in surface waters of the Western Antarctic Peninsula shelf. Mar. Chem. **196**: 81–97. doi:10.1016/j.marchem.2017.06.004

Behrenfeld, M. J., et al. 2009. Satellite-detected fluorescence reveals global physiology of ocean phytoplankton. Biogeosciences **6**: 779–794. doi:10.5194/bg-6-779-2009

Behrenfeld, M. J., and Z. S. Kolber. 1999. Widespread iron limitation of phytoplankton in the south pacific ocean. Science **283**: 840–843. doi:10.1126/science.283.5403.840

Behrenfeld, M. J., and A. J. Milligan. 2013. Photophysiological expressions of iron stress in phytoplankton. Ann. Rev. Mar. Sci. **5**: 217–246. doi:10.1146/annurev-marine-121211-172356

Bibby, T. S., M. Y. Gorbunov, K. W. Wyman, and P. G. Falkowski. 2008. Photosynthetic community responses to upwelling in mesoscale eddies in the subtropical North Atlantic and Pacific Oceans. Deep-Sea Res. Part II **55**: 1310–1320. doi:10.1016/j.dsr2.2008.01.014

Blanco-Ameijeiras, S., S. A. M. Moisset, S. Trimborn, D. A. Campbell, J. P. Heiden, and C. S. Hassler. 2018. Elemental stoichiometry and photophysiology regulation of *Synechococcus* sp. PCC7002 under increasing severity of chronic iron limitation. Plant Cell Physiol. **59**: 1803–1816. doi:10.1093/pcp/pcy097

Bonnet, S., and others. 2008. Nutrient limitation of primary productivity in the Southeast Pacific (BIOSOPE cruise). Biogeosciences **5**: 215–225. doi:10.5194/bg-5-215-2008

Boyd, P. W. 2002. Environmental factors controlling phytoplankton processes in the Southern Ocean. J. Phycol. **38**: 844–861. doi:10.1046/j.1529-8817.2002.t01-1-01203.x

Brody, S. S. 2002. Fluorescence lifetime, yield, energy transfer and spectrum in photosynthesis, 1950-1960. Photosynth. Res. **73**: 127–132. doi:10.1023/A:1020405921105, 1/3

Brody, S. S., and E. Rabinowitch. 1957. Excitation lifetime of photosynthetic pigments in vitro and in vivo. Science **125**: 555. doi:10.1126/science.125.3247.555

Buck, J. M., and others. 2019. Lhcx proteins provide photoprotection via thermal dissipation of absorbed light in the diatom *Phaeodactylum tricornutum*. Nat. Commun. **10**: 4167. doi:10.1038/s41467-019-12043-6

Butler, W. L. 1978. Energy distribution in the photochemical apparatus of photosynthesis. Annu. Rev. Plant Physiol. **29**: 345–378. doi:10.1146/annurev.pp.29.060178.002021

Butler, W. L., and R. J. Strasser. 1977. Tripartite model for the photochemical apparatus of green plant photosynthesis. Proc. Natl. Acad. Sci. **74**: 3382–3385. doi:10.1073/pnas.74.8.3382

Carvalho, F., and others. 2019. Testing the canyon hypothesis: Evaluating light and nutrient controls of phytoplankton growth in penguin foraging hotspots along the West Antarctic Peninsula. Limnol. Oceanogr. **1–16**: 455–470. doi:10.1002/lno.11313

Carvalho, F., J. Kohut, M. J. Oliver, and O. Schofield. 2017. Defining the ecologically relevant mixed-layer depth for Antarctica's coastal seas. Geophys. Res. Lett. **44**: 338–345. doi:10.1002/2016GL071205

Coale, K. H., and others. 2004. Southern ocean iron enrichment experiment: Carbon cycling in high- and low-Si waters. Science **304**: 408–414. doi:10.1126/science.1089778

Enderlein, J., and R. Erdmann. 1997. Fast fitting of multi-exponential decay curves. Opt. Commun. **134**: 371–378. doi:10.1016/S0030-4018(96)00384-7

Falkowski, P. G. 1994. The role of phytoplankton photosynthesis in global biogeochemical cycles. Photosynth. Res. **39**: 235–258. doi:10.1007/BF00014586

Falkowski, P. G., M. Koblížk, M. Gorbunov, and Z. Kolber. 2004. Development and application of variable chlorophyll fluorescence techniques in marine ecosystems, p. 757–778. *In* G. C. Papageorgiou and Govindjee [eds.], Chlorophyll a fluorescence: A signature of photosynthesis. the Netherlands: Springer.

Falkowski, P. G., H. Lin, and M. Y. Gorbunov. 2017. What limits photosynthetic energy conversion efficiency in nature? Lessons from the oceans. Philos. Trans. R. Soc. B Biol. Sci. **372**: 20160376. doi:10.1098/rstb.2016.0376

Falkowski, P. G., and J. A. Raven. 2014. Aquatic photosynthesis, 2nd ed. Princeton Univ. Press.

Gervais, F., U. Riebesell, and M. Y. Gorbunov. 2002. Changes in primary productivity and chlorophyll a in response to iron fertilization in the southern polar frontal zone. Limnol. Oceanogr. **47**: 1324–1335. doi:10.4319/lo.2002.47.5.1324

Gorbunov, M. Y., and P. G. Falkowski. 2005. Fluorescence induction and relaxation (FIRe) technique and instrumentation for monitoring photosynthetic processes and primary production in aquatic ecosystems. Photosynthesis: Fundamental Aspects to Global Perspectives. 13th Int. Congr. Photosynth. **2**: 1029–1031.

Gorbunov, M. Y., P. G. Falkowski, and Z. S. Kolber. 2000. Measurement of photosynthetic parameters in benthic organisms in situ using a SCUBA-based fast repetition rate fluorometer. Limnol. Oceanogr. **45**: 242–245.

Gorbunov, M. Y., Z. S. Kolber, M. P. Lesser, and P. G. Falkowski. 2001. Photosynthesis and photoprotection in symbiotic corals. Limnol. Ocean. **46**: 75–85.

Goss, R., and B. Lepetit. 2015. Biodiversity of NPQ. J. Plant Physiol. **172**: 13–32. doi:10.1016/j.jplph.2014.03.004

Greene, R. M., R. J. Geider, and P. G. Falkowski. 1991. Effect of iron limitation on photosynthesis in a marine diatom. Limnol. Oceanogr. **36**: 1772–1782. doi:10.4319/lo.1991.36.8.1772

Greene, R. M., R. J. Geider, Z. Kolber, and P. G. Falkowski. 1992. Iron-induced changes in light harvesting and photochemical energy conversion processes in eukaryotic marine algae. Plant Physiol. **100**: 565–575. doi:10.1104/pp.100.2.565

Greene, R. M., Z. S. Kolber, D. G. Swift, N. W. Tindale, and P. G. Falkowski. 1994. Physiological limitation of phytoplankton photosynthesis in the eastern equatorial Pacific determined from variability in the quantum yield of fluorescence. Limnol. Oceanogr. **39**: 1061–1074. doi:10.4319/lo.1994.39.5.1061

Hendrickson, L., R. T. Furbank, and W. S. Chow. 2004. A simple alternative approach to assessing the fate of absorbed light energy using chlorophyll fluorescence. Photosynth. Res. **82**: 73–81. doi:10.1023/B:PRES.0000040446.87305.f4

Ho, T. Y., A. Quigg, Z. V. Finkel, A. J. Milligan, K. Wyman, P. G. Falkowski, and F. M. M. Morel. 2003. The elemental composition of some marine phytoplankton. J. Phycol. **39**: 1145–1159. doi:10.1111/j.0022-3646.2003.03-090.x

Hopkinson, B. M., and others. 2007. Iron limitation across chlorophyll gradients in the southern Drake Passage: Phytoplankton responses to iron addition and photosynthetic indicators of iron stress. Limnol. Oceanogr. **52**: 2540–2554. doi:10.4319/lo.2007.52.6.2540

Huot, Y., C. A. Brown, and J. J. Cullen. 2005. New algorithms for MODIS sun-induced chlorophyll fluorescence and a comparison with present data products. Limnol. Oceanogr.: Methods **3**: 108–130. doi:10.4319/lom.2005.3.108

Hutchins, D. A., and others. 2002. Phytoplankton iron limitation in the Humboldt current and Peru upwelling. Limnol. Oceanogr. **47**: 997–1011. doi:10.4319/lo.2002.47.4.0997

Jassby, A. D., and T. Platt. 1976. Mathematical formulation of the relationship between photosynthesis and light for phytoplankton. Limnol. Oceanogr. **21**: 540–547. doi:10.4319/lo.1976.21.4.0540

Kolber, Z. S., O. Prášil, and P. G. Falkowski. 1998. Measurements of variable chlorophyll fluorescence using fast repetition rate techniques: Defining methodology and experimental protocols. Biochim. Biophys. Acta **1367**: 88–106. doi:10.1016/S0005-2728(98)00135-2

Kramer, D. M., G. Johnson, O. Kiirats, and G. E. Edwards. 2004. New fluorescence parameters for the determination of QA redox state and excitation energy fluxes. Photosynth. Res. **79**: 209–218. doi:10.1023/B:PRES.0000015391.99477.0d

Kuzminov, F. I., and M. Y. Gorbunov. 2016. Energy dissipation pathways in photosystem 2 of the diatom, *Phaeodactylum tricornutum*, under high-light conditions. Photosynth. Res. **127**: 219–235. doi:10.1007/s11120-015-0180-3

Lakowicz, J. R. 2006. Principles of fluorescence spectroscopy, 3rd ed. Springer.

Lepetit, B., and others. 2017. The diatom *Phaeodactylum tricornutum* adjusts nonphotochemical fluorescence quenching capacity in response to dynamic light via fine-tuned Lhcx and xanthophyll cycle pigment synthesis. New Phytol. **214**: 205–218. doi:10.1111/nph.14337

Ley, A. C., and D. C. Mauzerall. 1982. Absolute absorption cross-sections for photosystem II and the minimum quantum requirement for photosynthesis in *Chlorella vulgaris*. Biochim. Biophys. Acta **680**: 95–106. doi:10.1016/0005-2728(82)90320-6

Leys, C., C. Ley, O. Klein, P. Bernard, and L. Licata. 2013. Detecting outliers: Do not use standard deviation around the mean, use absolute deviation around the median. J. Exp. Soc. Psychol. **49**: 764–766.

Lin, H., F. I. Kuzminov, J. Park, S. Lee, P. G. Falkowski, and M. Y. Gorbunov. 2016. The fate of photons absorbed by phytoplankton in the global ocean. Science **351**: 264–267. doi:10.1126/science.aab2213

Macey, A. I., T. Ryan-Keogh, S. Richier, C. M. Moore, and T. S. Bibby. 2014. Photosynthetic protein stoichiometry and photophysiology in the high latitude North Atlantic. Limnol. Oceanogr. **59**: 1853–1864. doi:10.4319/lo.2014.59.6.1853

Moline, M. A. 1998. Photoadaptive response during the development of a coastal Antarctic diatom bloom and relationship to water column stability. Limnol. Oceanogr. **43**: 146–153. doi:10.4319/lo.1998.43.1.0146

Moline, M., B. Prezelin, and H. Claustre. 1996. Light-saturated primary production in Antarctic Coastal Waters. Antarct. J. United States **31**: 105.

Moore, C. M., and others. 2013. Processes and patterns of oceanic nutrient limitation. Nat. Geosci. **6**: 701–710. doi:10.1038/ngeo1765

Moore, C. M., S. Seeyave, A. E. Hickman, J. T. Allen, M. I. Lucas, H. Planquette, R. T. Pollard, and A. J. Poulton. 2007. Iron-light interactions during the CROZet natural iron bloom and EXport experiment (CROZEX) I: Phytoplankton growth and photophysiology. Deep-Sea Res. Part II Top. Stud. Oceanogr. **54**: 2045–2065. doi:10.1016/j.dsr2.2007.06.011

Nelson, D. M., and W. Smith. 1991. The role of light and major nutrients. Limnol. Oceanogr. **36**: 1650–1661.

Owens, T. G. 1986. Light-harvesting function in the diatom *Phaeodactylum tricornutum*. Plant Physiol. **80**: 739–746. doi:10.1104/pp.80.3.739

Palacios, M. A., F. L. De Weerd, J. A. Ihalainen, R. Van Grondelle, and H. Van Amerongen. 2002. Superradiance and exciton (de)localization in light-harvesting complex II from green plants? J. Phys. Chem. B **106**: 5782–5787. doi:10.1021/jp014078t

Park, J., F. I. Kuzminov, B. Bailleul, E. J. Yang, S. H. Lee, P. G. Falkowski, and M. Y. Gorbunov. 2017. Light availability rather than Fe controls the magnitude of massive phytoplankton bloom in the Amundsen Sea polynyas, Antarctica. Limnol. Oceanogr. **62**: 2260–2276. doi:10.1002/lno.10565

Petrou, K., C. S. Hassler, M. A. Doblin, K. Shelly, V. Schoemann, R. van den Enden, S. Wright, and P. J. Ralph. 2011. Iron-limitation and high light stress on phytoplankton populations from the Australian sub-Antarctic zone (SAZ). Deep-Sea Res. Part II Top. Stud. Oceanogr. **58**: 2200–2211. doi:10.1016/j.dsr2.2011.05.020

Ralph, P. J., and R. Gademann. 2005. Rapid light curves: A powerful tool to assess photosynthetic activity. Aquat. Bot. **82**: 222–237. doi:10.1016/j.aquabot.2005.02.006

Ryan-Keogh, T. J., L. M. DeLizo, W. O. Smith, P. N. Sedwick, D. J. McGillicuddy, C. M. Moore, and T. S. Bibby. 2017. Temporal progression of photosynthetic-strategy in phytoplankton in the Ross Sea. Antarctica. J. Mar. Syst. **166**: 87–96. doi:10.1016/j.jmarsys.2016.08.014

Schallenberg, C., R. F. Strzepek, N. Schuback, L. A. Clementson, P. W. Boyd, and T. W. Trull. 2020. Diel quenching of Southern Ocean phytoplankton fluorescence

is related to iron limitation. Biogeosciences **17**: 793–812. doi:10.5194/bg-17-793-2020

Schofield, O., M. Brown, J. Kohut, S. Nardelli, G. Saba, N. Waite, and H. Ducklow. 2018. Changes in the upper ocean mixed layer and phytoplankton productivity along the West Antarctic Peninsula. Philos. Trans. R. Soc. A **376**: 20170173. doi:10.1098/rsta.2017.0173

Schofield, O., and others. 2017. Decadal variability in coastal phytoplankton community composition in a changing West Antarctic peninsula. Deep-Sea Res. Part I Oceanogr. Res. Pap. **124**: 42–54. doi:10.1016/j.dsr.2017.04.014

Schrader, P. S., A. J. Milligan, and M. J. Behrenfeld. 2011. Surplus photosynthetic antennae complexes underlie diagnostics of iron limitation in a cyanobacterium. PLoS One **6**: 18753. doi:10.1371/journal.pone.0018753

Schuback, N., C. Schallenberg, C. Duckham, M. T. Maldonado, and P. D. Tortell. 2015. Interacting effects of light and iron availability on the coupling of photosynthetic electron transport and CO_2-assimilation in marine phytoplankton. PLoS One **10**: 1–30. doi:10.1371/journal.pone.0133235

Serôdio, J., S. Vieira, S. Cruz, and H. Coelho. 2006. Rapid light-response curves of chlorophyll fluorescence in microalgae: Relationship to steady-state light curves and non-photochemical quenching in benthic diatom-dominated assemblages. Photosynth. Res. **90**: 29–43. doi:10.1007/s11120-006-9105-5

Steinberg, D. K., and others. 2015. Long-term (1993-2013) changes in macrozooplankton off the western antarctic peninsula. Deep-Sea Res. Part I Oceanogr. Res. Pap. **101**: 54–70. doi:10.1016/j.dsr.2015.02.009

Strzepek, R. F., P. W. Boyd, and W. G. Sunda. 2019. Photosynthetic adaptation to low iron, light, and temperature in Southern Ocean phytoplankton. Proc. Natl. Acad. Sci. USA **116**: 4388–4393. doi:10.1073/pnas.1810886116

Strzepek, R. F., K. A. Hunter, R. D. Frew, P. J. Harrison, and P. W. Boyd. 2012. Iron-light interactions differ in Southern Ocean phytoplankton. Limnol. Oceanogr. **57**: 1182–1200. doi:10.4319/lo.2012.57.4.1182

Suggett, D. J., S. Goyen, C. Evenhuis, M. Szabó, D. T. Pettay, M. E. Warner, and P. J. Ralph. 2015. Functional diversity of photobiological traits within the genus *Symbiodinium* appears to be governed by the interaction of cell size with cladal designation. New Phytol. **208**: 370–381. doi:10.1111/nph.13483

Suggett, D. J., C. M. Moore, A. E. Hickman, and R. J. Geider. 2009. Interpretation of fast repetition rate (FRR) fluorescence: Signatures of phytoplankton community structure versus physiological state. Mar. Ecol. Prog. Ser. **376**: 1–19. doi:10.3354/meps07830

Suzuki, K., H. Liu, T. Saino, H. Obata, M. Takano, K. Okamura, Y. Sohrin, and Y. Fujishima. 2002. East-west gradients in the photosynthetic potential of phytoplankton and iron concentration in the subarctic Pacific Ocean during early summer. Limnol. Oceanogr. **47**: 1581–1594. doi:10.4319/lo.2002.47.6.1581

Sverdrup, H. U. 1953. On the conditions of the vernal blooming of phytoplankton. J. Cons. Int. Éxplor. Mer. **18**: 287–295.

Vassiliev, I. R., Z. Kolber, K. D. Wyman, D. Mauzerall, V. K. Shukla, and P. G. Falkowski. 1995. Effects of iron limitation on photosystem II composition and light utilization in *Dunaliella tertiolecta*. Plant Physiol. **109**: 963–972. doi:10.1104/pp.109.3.963

Waters, K. J., and R. C. Smith. 1992. Palmer LTER: A sampling grid for the Palmer LTER program. Antarct. J. United States **27**: 236–239.

Wientjes, E., H. Van Amerongen, and R. Croce. 2013. Quantum yield of charge separation in photosystem II: Functional effect of changes in the antenna size upon light acclimation. J. Phys. Chem. B **117**: 11200–11208. doi:10.1021/jp401663w

Acknowledgments

The authors thank the crew and support staff of ARSV Laurence M. Gould during LMG17-01. We also thank Schuyler Nardelli and Naomi Shelton for help analyzing chlorophyll and nutrient concentrations, Robert Sherell and Kevin Wyman for comments on the manuscript, and two anonymous reviewers and Editor for constructive comments. This research was supported by NASA Ocean Biology and Biogeochemistry Program (grants NNX16AT54G and 80NSSC18K1416 to M.Y.G. and P.G.F.) and LTER Program of the US National Science Foundation (ANT-0823101 to O.S.). J.S. is supported by a graduate fellowship from the Department of Marine and Coastal Sciences at Rutgers University.

Conflict of interest

None declared.

Submitted 23 December 2019
Revised 18 April 2020
Accepted 23 June 2020

Associate editor: Heidi Sosik